ICLASS 2009, 11th Triennial International Annual Conference on Liquid Atomization and Spray Systems, Vail, Colorado USA, July 2009

Detailed Simulations of the Breakup Processes of Turbulent Liquid Jets in Subsonic Crossflows

M. Herrmann*
Department of Mechanical and Aerospace Engineering, Arizona State University
Tempe, Arizona 85287,USA

Abstract

This paper presents numerical simulation results of the primary atomization of a turbulent liquid jet injected into a gaseous crossflow. Simulations are performed using the balanced force Refined Level Set Grid method. The phase interface during the initial breakup phase is tracked by a level set method on a separate refined grid. A balanced force finite volume algorithm together with an interface projected curvature evaluation is used to ensure the stable and accurate treatment of surface tension forces even on small scales. Broken off, small scale nearly spherical drops are transferred into a Lagrangian point particle description allowing for full two-way coupling and continued secondary atomization. The numerical method is applied to the simulation of the primary atomization region of a turbulent liquid jet (q=6.6, We=330, Re=14,000) injected into a gaseous crossflow (Re=570,000), analyzed experimentally by Brown and McDonell (2006). The simulations take the actual geometry of the injector into account. Grid converged simulation results of the jet penetration agree well with experimentally obtained correlations. Both column/bag breakup and shear/ligament breakup modes can be observed on the liquid jet. A grid refinement study shows that on the finest employed grids (flow solver 64 points per injector diameter, level set solver 128 points per injector diameter), grid converged drop sizes are achieved for drops as small as one-hundredth the size of the injector diameter.

Introduction

The atomization of turbulent liquid jets injected into fast moving, subsonic gaseous crossflows is an important application for example in gas turbines, ramjets, and augmentors. It is a highly complex process, that has been extensively studied experimentally over the past decades. Early studies of the atomization of non-turbulent liquid jets in crossflows have recently been reviewed in [1], whereas newer studies of this case include the work reported in [1–7]. Most experimental work has focused on jet penetration, including both the column trajectory and the resulting spray penetration. Some recent jet penetration correlations can be found in [3, 7]. Experimental studies of non-turbulent liquid jets injected into subsonic crossflows have concluded, that depending on the momentum flux ratio q and crossflow Weber number We_c, essentially two different breakup modes can be observed [7]. For low q and We_c, the liquid jet breaks up as a whole some distance downstream of the injector. For high q and We_c, on the other hand, surface breakup or stripping at the sides of the liquid jets is observed prior to column breakup [7]. Unlike nonturbulent jets, turbulent liquid jets do not exhibit this clear separation of breakup modes [8]. Stripping at the sides of the liquid column occurs even at low Weber numbers, where non-turbulent jets exhibit only the column breakup mode. Turbulence initiates the generation of ligaments that then break up due to the Raleigh mechanism [8].

Modeling attempts of the atomization process have had mixed results. While correlations for jet penetration derived from experimental data give good agreement for parameter ranges and configurations for which they were developed, numerical simulations predicting the jet penetration, drop sizes and liquid volume fluxes have had mixed success [1, 9, 10]. This is in part due to the fact that under most operating conditions, turbulence interaction is strong and several different atomization mechanisms occur on the jet's surface at the same time. Detailed numerical simulations, as presented in this paper, can help study these simultaneously occurring mechanisms, even in regions of the liquid jet, where traditional experimental methods cannot observe the phase interface dynamics [11]. However, although detailed simulations solve the Navier-Stokes equations directly, it is incumbent on any numerical simulation to demonstrate that spatial and temporal discretization errors are not unduly impacting the obtained results.

*Corresponding Author: marcus.herrmann@asu.edu

	exp.	sim.
jet exit diameter D [mm]	1.3	1.3
crossflow density ρ_c [kg/m^3]	1.225	1.225
jet density ρ_j [kg/m^3]	1000	12.25
crossflow velocity u_c [m/s]	120.4	120.4
jet velocity u_j [m/s]	10.83	97.84
crossflow viscosity μ_c [kg/ms]	1.82e-5	1.82 e-5
jet viscosity μ_j [kg/ms]	1.0e-3	1.11e-4
surface tension coeff. σ [N/m]	0.07	0.07

	exp.	sim.
momentum flux ratio q	6.6	6.6
crossflow Weber We$_c$	330	330
jet Weber We$_j$	2178	2178
crossflow Reynolds Re$_c$	5.7e5	5.7e5
jet Reynolds Re$_j$	14079	14079

Table 1. Operating conditions and characteristic numbers.

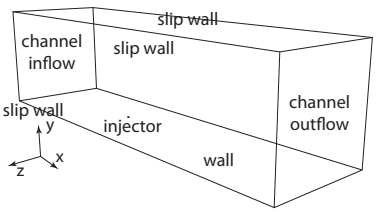

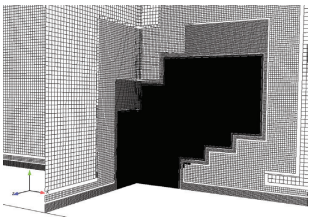

case	c01	c12	c23
fs min Δx	$D/16$	$D/32$	$D/64$
RLSG Δx_G	$D/32$	$D/64$	$D/128$
fs mesh size	8.7e6	21e6	110e6
RLSG max mesh	3.5e6	13e6	66e6

Figure 1. Computational domain and boundary conditions (left), mesh detail near the injector (center), and grid resolution and mesh sizes (right).

Numerical methods

In this work we use the flow solver CDP/CHARLES that solves the incompressible two-phase Navier-Stokes equations on unstructured grids using the finite volume balanced force algorithm [12]. In the single phase regions, the employed scheme conserves the kinetic energy discretely. Turbulence in the single phase regions of the flow is modeled using a dynamic Smagorinsky LES model, however, none of the terms arising from filtering the phase interface are modeled. The approach instead relies on resolving all relevant scales at the phase interface, thus ideally reverting to a DNS there.

The liquid/gas phase interface during primary atomizaton is tracked by the interface tracking software LIT, using the Refined Level Set Grid method [12]. This solver uses a fifth-order WENO scheme [13] in conjunction with a third order TVD Runge-Kutta time discretization [14].

Tracked small scale nearly spherical separated liquid structures are transferred from the level set description into a Lagrangian point particle/parcle model [15] using a parallel multi-scale coupling procedure [16]. In the Lagrangian description, full two-way momentum coupling between the drop and continuous phase is used, including a stochastic secondary atomization model [17].

Computational Domain and Operating Conditions

The case analyzed in this paper is one studied experimentally by Brown & McDonell [2]. Table 1 summarizes the operating conditions and resulting characteristic numbers. Note that although the density ratio is artificially reduced from the experimental values, all relevant characteristic numbers, i.e., momentum flux ratio q, crossflow Weber number We$_c$, jet Weber number We$_j$, crossflow Reynolds number Re$_c$, and jet Reynolds number Re$_j$, are the same as in the experiment. Figure 1 depicts the computational domain of size $-25D \ldots 50D \times 0 \ldots 25D \times -10D \ldots 10D$ and the used boundary conditions as well as a zoom into the near-injector region to show the mesh detail used in the simulations.

In a first step, detailed single phase LES of the experimentally used injector geometry and crossflow channel in the vicinity of the injector exit were performed using a dynamic Smagorinsky model, matching the correct experimental momentum flux ratio and Reynolds number, see Tab. 1. Inflow boundary conditions into the injector were taken from a pre-computed LES pipe flow simulation database at the appropriate Reynolds number. The injector exit plane velocity distributions were then stored as a time sequence in a database to be used in the subsequent two-phase atomization simulations.

The two-phase atomization simulations were performed using three different grids of increasing resolution in order to address the important question of how much the employed grid resolution impacts the atomization results. Figure 1 summarizes the meshes employed in the three cases c01, c12, and c23. The flow solver grid consists of hexahedra of edge length $D/4$, which are isotropically refined in layers near the injector and

lower channel walls, such that the spatial region where the phase interface is tracked is completely filled with equidistant grid cells of the minimum cell size Δx reported in Fig. 1. In each case, the G-grid is a factor 2 finer than the flow solver grid in order to enhance numerical accuracy of the interface tracking scheme.

Results and Discussion

Figure 2 shows the temporal evolution of the level set tracked liquid mass for the three different grid resolutions. All cases show an initial linear increase. This is due to the fact that at this early stage, almost no small scale drops are generated that would be transferred out of the tracked and into the Lagrangian representation. Then at around $t = 5$, significant numbers of small scale drops that fulfill the transfer

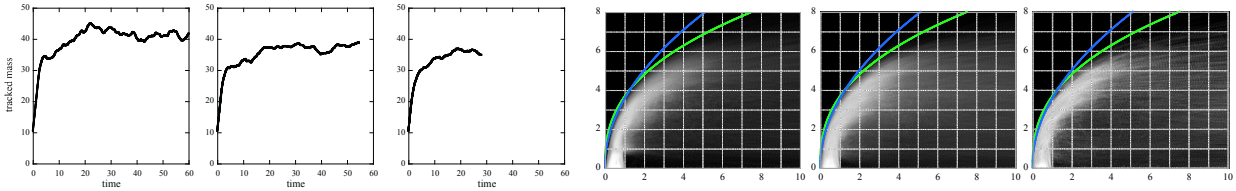

Figure 2. Temporal evolution of tracked liquid mass (left) and averaged jet penetration side view for different grid resolutions (from left to right in each: c01, c12, and c23) with jet penetration correlations due to Wu et al. [7] (blue) and Stenzler et al.[3] (green).

criterium start to be generated resulting in a slower increase in the tracked mass until at around $t = 20$ a statistically steady state is reached. From this point on, a balance exists between the injected liquid mass and the atomized liquid mass that is transferred into the Lagrangian description. It is interesting to note that the coarse grid simulation c01 tends to a larger value of the tracked liquid mass, whereas the two higher resolution cases result in slightly smaller, but similar values. This appears to be due to the fact that for the coarse grid simulations, small scale unresolved turbulent eddies cannot initiate atomization, thus resulting in a smaller transfer rate per phase interface area. The higher resolution cases, on the other hand do resolve significantly more small scale turbulent eddies that can corrugate the interface and thus initiate atomization quicker. This conjecture is supported by analyzing the instantaneous phase interface geometries shown in Fig. 3 that show significantly more small scale structures with increasing grid resolution. Since Fig. 2 indicates that a steady state is reached for $t > 20$, all statistics presented in the following are evaluated only for $t > 20$ for a total of 43 time units for case c01, 35 time units for case c12, and 8.1 time units for case c23.

Figure 2 also shows an averaged side view of the atomizing liquid jets evaluated for $t > 20$. The jet penetration is compared to the predictions of two common correlations for the penetration of the upper edge of the liquid jet derived by fitting experimental data due to Wu et al. [7] (shown in blue) and Stenzler et al. [3] (shown in green). Recent experimental observations reported in [2] show better agreement with the correlation due to Stenzler et al. [3] which is the case in the simulation results as well. Note that there is virtually no difference between the three different resolution cases, indicating that even for coarse grids, good jet penetration results can be obtained.

Figure 3 show snapshots of the atomizing liquid jets at different times and different grid resolutions viewed from the side and front. Two main simultaneous atomization mechanisms can be observed. All cases show instability waves being generated, predominantly visible on the windward side. These instabilities generate role-ups and continue to grow along the jet axis until they form bag like structures that rupture resulting in a broad range of drop sizes, not unlike the column-breakup mode. It is speculated that this instability mode is due to a Kelvin-Helmholtz instability, however, this conjecture is still to be verified using the generated simulation data. The larger scale instability mode is most clearly visible in the lowest resolution case c01. It is equally present in the higher resolution cases, but there it is overlaid by significant turbulence induced surface corrugations and thus not as visibly pronounced.

In addition to the conjectured column breakup mode, ligaments are formed at the sides of the liquid jets near the injector exit that stretch out and then break up forming a range of drop sizes. Figure 4 shows a time sequence of such ligament breakups in the c01 case. Corrugations on the liquid jet surface, likely generated initially by turbulent eddies present in the liquid jet, are stretched out into ligaments. This mechanism has been observed recently as well in detailed simulations of turbulent liquid jets injected into still air [18]. In laminar liquid jets atomized by fast moving co-flowing gas, ligament formation and stretching is also observed and attributed to a Rayleigh-Taylor mechanism [19]. The stretched out ligaments then seem to

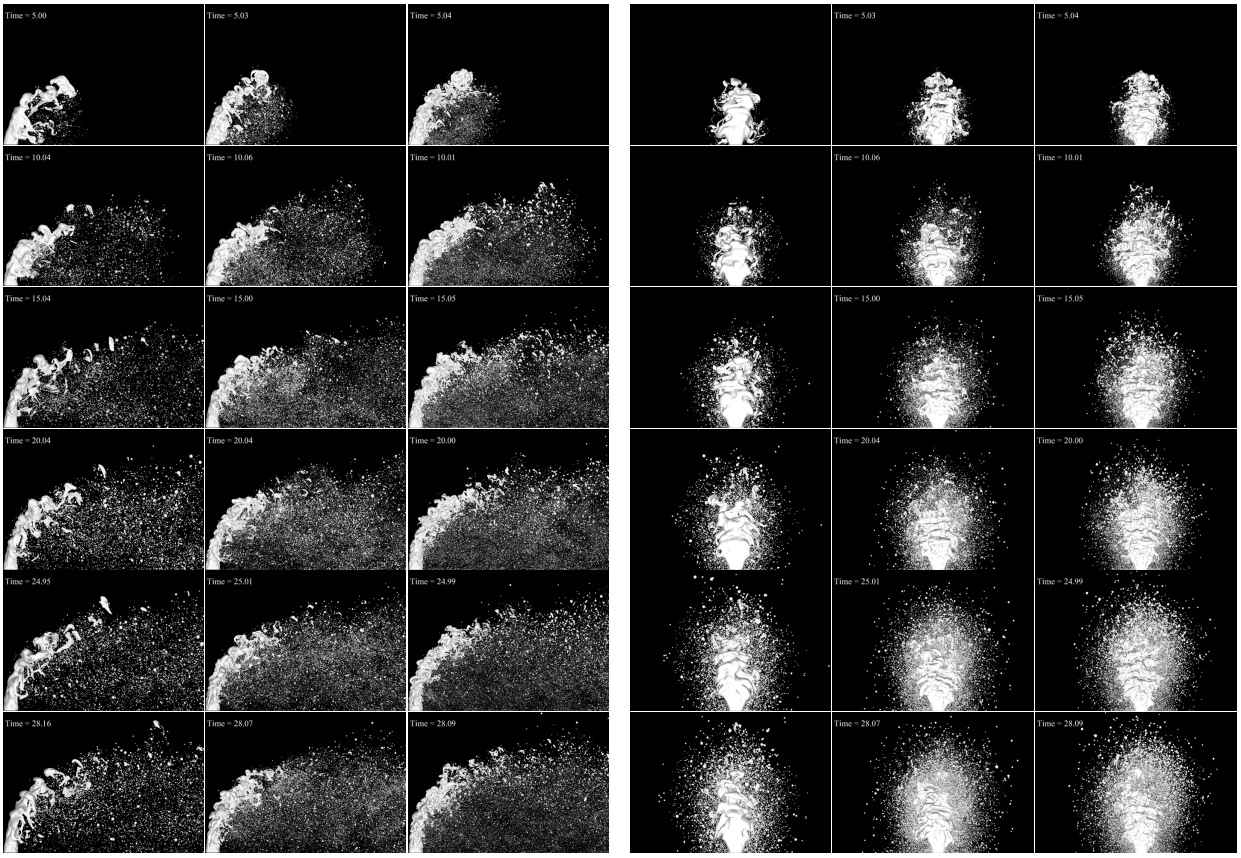

Figure 3. Side and front view snapshots of jet in crossflow atomization at t=5, 10, 15, 20, 25, and 28.1 time units (top to bottom). case c01 (left), c12 (center), and c23 (right).

break up due to a Rayleigh mechanism, as proposed in [8]. At the current stage, the above description of the breakup mechanism is speculative and still requires a detailed, yet to be performed, quantitative study of the generated time dependent simulation data.

Note that due to the turbulent (chaotic) nature of the flow, it cannot be expected that the instantaneous phase interface geometry shown in Fig. 3 converges under grid refinement. Only statistical quantities like the mean jet penetration or the drop size distribution should converge. However, it can be seen, that many of the larger scale structures on the liquid jet appear to be similar for all three grid resolutions, indicating that the large scale instability mode generated on the upstream pointing side of the liquid jet might be deterministic and sufficiently resolved even on the coarser grids. However, the higher resolution cases show significantly more fine scale structure on the liquid jet.

Besides mean jet penetration and observed breakup modes, the key quantity to ascertain the quality of a numerical simulation is the grid dependency/independency of the resulting atomized drop size distribution. Figure 5 depicts the calculated drop size distributions obtained from primary atomization at $t > 20$ for the three different grid resolutions analyzed in this study. Shown are only those drops that are generated directly from the liquid jet, i.e., drops that are transferred from the level set tracked phase interface representation to the Lagrangian point particle description. Note that these drops can continue to atomize via secondary atomization mechanisms further downstream, however, within the computational domain, only a limited number of these secondary atomization events occur.

The drop size distributions were generated by binning the data into 20 bins of equal size in terms of $\log(d)$. The approximate total number of drops used to calculate each distribution was 40,000 (c01), 176,000 (c12), and 193,000 (c23). To be able to compare the three pdfs, the coarser grid pdfs were normalized using a single bin of the finest grid pdf. Also shown in Fig. 5 is a log-normal fit to the larger drop sizes of the finest grid results. All three cases show a similar behavior. Larger drop sizes collapse well to the log-normal fit, however, for each grid, there is a distinct departure point from the fit, from which point on, smaller drop sizes do not collapse and fail to match the log-normal fit. This departure point d_p is decreasing

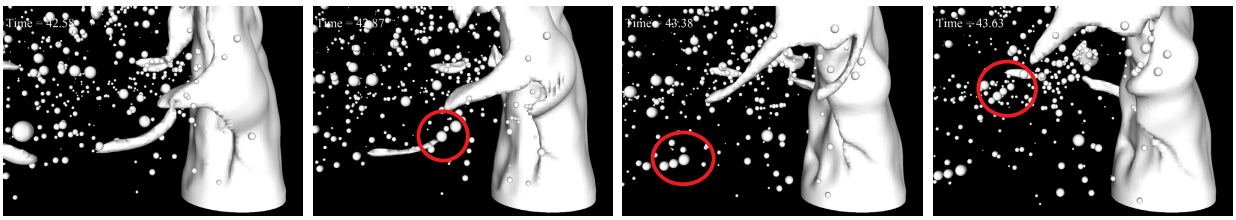

Figure 4. Time sequence of ligament breakup mode (red circled regions indicate ligament generated drops); case c01. Time advances from top left to bottom right.

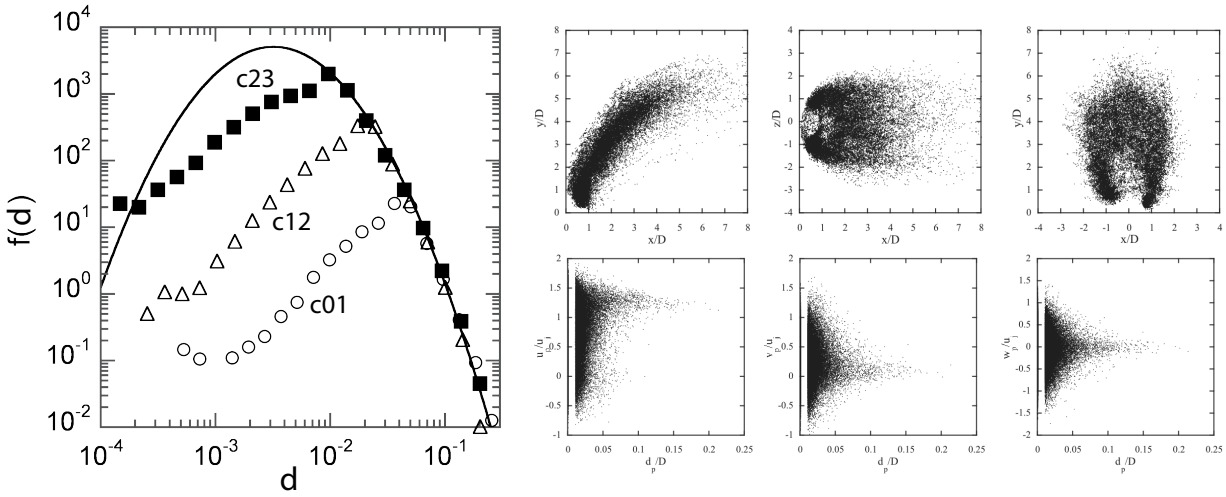

Figure 5. Grid convergence study of pfd of drop diameters d with solid line log-normal fit to large drop sizes of c23 (left); case c23 transferred drop positions (right top: side, top, and front view), and drop velocities as function of drop size (right bottom: crossflow, jet, and transverse direction).

in value proportional to the employed grid size, with $d_p = 1.6\Delta x_G$ for the coarse and medium grid and $d_p = 1.3\Delta x_G$ for the fine grid. The key result here is the fact that larger drops, i.e., those resolved by at least 1.6 G-grid cells, collapse to a single pdf, in this case a log-normal distribution, independent of the employed grid resolution. These drop sizes can thus be considered grid-independent. Drops smaller than about $d = 1.6\Delta x_G$, however, show a strong grid dependency. The reason for this behavior is the following: fixed grid methods used to track interfaces, like the level set method used here, have an inherent topology change length scale that is proportional to the local grid size. As soon as two front segments enter the same grid cell, a topology change event is automatically triggered. The exact moment of breakup is thus always a function of the employed grid size. However, for larger drops, the error introduced by missing the exact moment of breakup due to the inherent grid size dependency is small compared to the generated drop size. Thus larger drop sizes are grid independent as demonstrated in Fig. 5. For smaller drops, the exact moment of breakup is however the dominant source of error, thus smaller drops are dominated by the employed grid resolution. The cut-off appears to occur at drops resolved by about 1.6 G-grid cells. This number is surprisingly low and appears to decrease with increasing grid resolution. This seems to indicate that the numerically induced topology change starts to mimic the physical breakup mechanism on small scales.

Figure 5 also shows the position and velocity of drops that are considered to be grid converged at their moment of transfer from the tracked to the Lagrangian representation for case c23 and $t > 20$. This moment of transfer can be interpreted as the conclusion of the primary breakup process. Atomization seems to occur first at around $y/D = 0.2$. In the lower parts of the jet it is mostly confined to the sides of the jet with almost no atomization occuring on the lower part of the leeward side of the jet. Primary atomization, as defined above, appears to be mostly completed at around $x/D = 5$ and $y/D = 6$, indicated by the noticeable drop in generated drops. The slight asymmetry visible in the front view of Fig. 5 is due to the relatively short averaging time available in the highest resolution run c23.

Finally, Fig. 5 also shows the drop velocities at the moment of transfer as a function of drop size. Only drops that are considered to be grid converged are included. Small drops exhibit a broad range of crossflow-, jet-, and transverse-direction velocities, with some drops even moving upstream in the crossflow and jet

direction at the moment of transition. These small scale drops are for the most part being generated in or near the wake region of the liquid jet and are caught in larger scale turbulent eddies causing them to temporarily move upstream and downward. Larger scale drops appear to converge to a nearly constant velocity of about $u_p/u_j = 1.25$ in the crossflow direction, $v_p/u_j = 0.1$ in the jet direction, and $w_p/u_j = 0$ in the transverse direction, although more data is needed to perform adequate statistical analysis for these larger drops. The above values can be explained by the fact that large scale structures are subjected to significant drag forces and thus have accelerated significantly in the crossflow direction, decelerated significantly in the jet direction, and are not easily prone to transverse vortical structures due to their relative large inertia.

It should be pointed out that these velocity results are significantly different from the experimental observations for fully developed turbulent straight pipe injectors [8]. There, a nearly uniform velocity in the crossflow direction for all drop sizes at the moment of primary breakup is reported. While this appears to be the case for larger scale drops here, too, our results indicate that smaller drops are subject to significant variations in their velocity at the moment of primary breakup. This discrepancy for small drops is likely due to the chosen reduced density ratio and hence reduced Stokes number of the liquid structures.

While the reduced density ratio appears to have no significant impact on the jet penetration, it is conceivable that the resulting drop size distribution is a function of the chosen density ratio. Experimental results to that effect, albeit in the case of turbulent liquid jets injected in still ambient air, are reported in [20] and references therein. There, it is hypothesized that a reduction in density ratio below a value of 500 will reduce Sauter mean diameters due to an increase in the relative importance of the aerodynamic effect. An increase of the density ratio used in the current simulations to values closer to those used in [8] could thus produce larger drops that would exhibit a more uniform velocity distribution. Currently ongoing simulations employing such higher density ratios will answer these questions.

Acknowledgments

This work was supported in part by CASCADE Technologies Inc. under the NavAir SBIR N07-046. The author would like to thank S. Hajiloo and Y. Khalighi for valuable help in generating the fluid solver meshes, and F. Ham for many valuable discussions concerning the flow solver CDP/CHARLES.

References

[1] Aalburg, C., van Leer, B., et al. *Atom. Sprays* 15(3):271–294, 2005.
[2] Brown, C.T. and McDonell, V.G. In *ILASS Americas, 19th Annual Conference on Liquid Atomization and Spray Systems*. Toronto, Canada, 2006.
[3] Stenzler, J.N., Lee, J.G., et al. *Atom. Sprays* 16:887–906, 2006.
[4] Mazallon, J., Dai, Z., et al. *Atom. Sprays* 9(3):291–311, 1999.
[5] Sallam, K.A., Aalburg, C., et al. *AIAA J.* 42(12):2529–2540, 2004.
[6] Fuller, R.P., Wu, P.K., et al. *AIAA J.* 38(1):64–72, 2000.
[7] Wu, P.K., Kirkendall, K.A., et al. *J. Propul. Power* 13(1):64–73, 1997.
[8] Lee, K., Aalburg, C., et al. *AIAA J.* 45(8):1907–1916, 2007.
[9] Madabhushi, R.K. *Atom. Sprays* 13(4):413–424, 2003.
[10] Arienti, M., Madabhusi, R.K., et al. In *ILASS Americas 18th Annual Conference on Liquid Atomization and Spray Systems*. Irvine, CA, 2005.
[11] Gorokhovski, M. and Herrmann, M. *Annual Review of Fluid Mechanics* 40(1):343–366, 2008.
[12] Herrmann, M. *J. Comput. Phys.* 227(4):2674–2706, 2008.
[13] Jiang, G.S. and Peng, D. *SIAM J. Sci. Comput.* 21(6):2126–2143, 2000.
[14] Shu, C.W. *SIAM J. Sci. Stat. Comput.* 9(6):1073–1084, 1988.
[15] Moin, P. and Apte, S.V. *AIAA J.* 44(4):698–708, 2006.
[16] Herrmann, M. In *ILASS Americas 19th Annual Conference on Liquid Atomization and Spray Systems*. ILASS Americas, Toronto, Canada, 2006.
[17] Apte, S.V., Gorokhovski, M., et al. *Int. J. Multiphase Flow* 29(9):1503–1522, 2003.
[18] Herrmann, M. In *ILASS Americas 21st Annual Conference on Liquid Atomization and Spray Systems*. Orlando, FL, 2008.
[19] Marmottant, P. and Villermaux, E. *J. Fluid Mech.* 498:73–111, 2004.
[20] Faeth, G.M., Hsiang, L.P., et al. *Int. J. Multiphase Flow* 21(Suppl. 1):99–127, 1995.